Interband $\Gamma_6 \rightarrow \Gamma_8$ Magnetoabsorption in HgTe

Y. Guldner and C. Rigaux
Groupe de Physique des Solides, Ecole Normale Supérieure, Paris, France

M. Grynberg
Institute of Experimental Physics, Warsaw University, Warsaw, Poland

A. Mycielski
Institute of Physics, P.A.N., Warsaw, Poland

(Received 7 March 1973)

Magnetoabsorption associated with $\Gamma_6 \rightarrow \Gamma_8$ transitions was investigated at 4.4 °K, on pure n-type HgTe thin crystals in the spectral region 300–400 meV for σ and π polarizations. Analysis of experimental spectra is performed using both the three-band model (including the nonparabolicity), and the theory of Luttinger. Band parameters are determined by fitting transition energies: $E_{\Gamma_8} - E_{\Gamma_6} = 302.5$ meV, $m_{\Gamma_6}/m_0 = 0.028 \pm 0.001$, and $g_{\Gamma_6} = -41 \pm 4$ at Γ. Γ_8 Luttinger parameters ($\gamma_1 = -12.8$, $\bar{\gamma} = -8.4$, $\kappa = -10.5$) satisfactorily explain interband and intraband Γ_8 magnetoabsorption. The structure of Γ_8 magnetic levels near Γ is quantitatively described by calculating the k_H dependence of the energies in the [111] direction. A complex structure is found for a set of heavy holes.

INTRODUCTION

HgTe exhibits the inverted band structure, theoretically predicted by Groves and Paul[1] for α-Sn. The band edges belonging to the zinc-blende space group T_d^2 are sixfold degenerate, including spin, at the center of the Brillouin zone. The spin-orbit interaction partially removes the degeneracy by lowering the two Γ_7 states ($J = \frac{1}{2}$) by $\Delta \simeq 1$ eV with respect to the four degenerate Γ_8 levels ($J = \frac{3}{2}$), representing both the top of the valence band and the bottom of the conduction band. The curvatures of the bands are mainly determined by $\vec{k} \cdot \vec{p}$ interaction between Γ_8 states (p type) and Γ_6 level (s type) lying below the degeneracy point (Fig. 1).

The evidence for the inverted structure of HgTe was first provided by measurements of thermoelectric power under hydrostatic pressure performed by Piotrzkowski *et al.*,[2] by optical-absorption experiments carried out by Mycielski and Galazka,[3] and by interband magnetoreflexion data obtained by Groves, Brown, and Pidgeon.[4,5]

Recent studies of intraband and interband magnetoabsorption were carried out at low temperature on n-type single crystals of HgTe, with low electronic concentration. This paper presents experimental results of $\Gamma_6 \rightarrow \Gamma_8$ magnetoabsorption investigated on very thin crystals (2 μm) in the infrared region $3 < \lambda < 4$ μm. The main purpose of this work was to study the Γ_8 band as well as the previously not experimentally investigated Γ_6 band.

Intraband Γ_8 magneto-optical data obtained by Tuchendler *et al.*[6] at submillimeter and far-infrared wavelengths are reported in the following paper.

Analysis of both interband $\Gamma_6 \rightarrow \Gamma_8$ and intraband Γ_8 experiments performed on the basis of the theory of Luttinger provides a quantitative description of Γ_8 magnetic levels. Γ_8 Luttinger parameters and the band-edge effective mass and gyromagnetic factor of the light holes are determined.

I. EXPERIMENTAL METHODS

A. Sample Preparation

The samples used in experiments were obtained by crystallization from a solution of tellurium in mercury.[3] Solution containing from 0.1–0.5 at.% tellurium was placed in a glass vial, which was pumped to the pressure of 10^{-5} torr and then sealed. The vial was placed in a horizontal furnace at temperature 450 °C and very slowly cooled down to room temperature. A thin layer of single crystals of HgTe was formed on the surface of the mercury. The thickness of this layer was 15–50 μm depending on the cooling conditions and the amount of tellurium. The proportions of mercury and tellurium in the plates obtained by this method are stoichiometric. The surfaces of the plates are mirrorlike and belong to the (111) plane.

The electron concentration and the mobilities were determined by galvanomagnetic measurements: at 4.2 °K, $n_e = (4-5) \times 10^{15}$ cm^{-3}, $\mu \sim 6 \times 10^5$ cm^2 V^{-1} sec^{-1}. Thin samples, 2 μm thick, required for transmission measurements, were prepared by chemical etching in bromine–methyl alcohol solution (4%).

B. Experimental Details

Magnetoabsorption experiments were performed at 4.4 °K in a superconducting magnet ($H \leq 60$ kG).

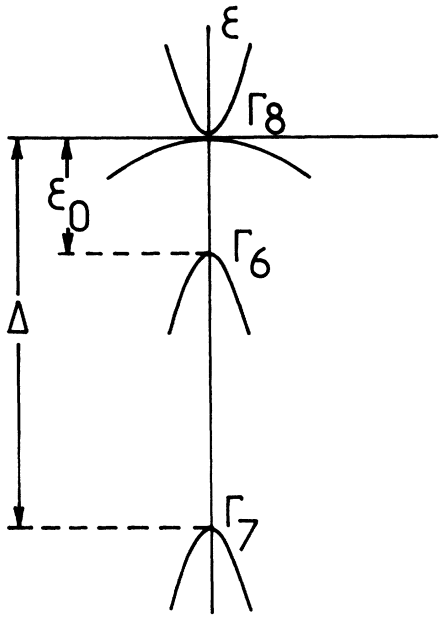

FIG. 1. Inverted band structure of HgTe.

The thin samples were freely mounted between two sapphire plates cut perpendicular to the c axis. The required resolution (about 1000) in the spectral energy range 300–400 meV was achieved by a grating monochromator and a cooled (77 °K) InSb photovoltaic detector.

The experiments were carried out in the Voigt configuration with linearly polarized radiation either parallel or perpendicular to the magnetic field, and in the Faraday configuration with circularly polarized light. In this case, the magnetic field was oriented along the [111] crystallographic direction. Circularly polarized radiation was obtained by a $\lambda/4$ plate of sapphire in conjunction with a wire-grid plane polarizer.

Magnetoabsorption data were taken by sweeping the magnetic field at fixed photon energy in the range 300–400 meV.

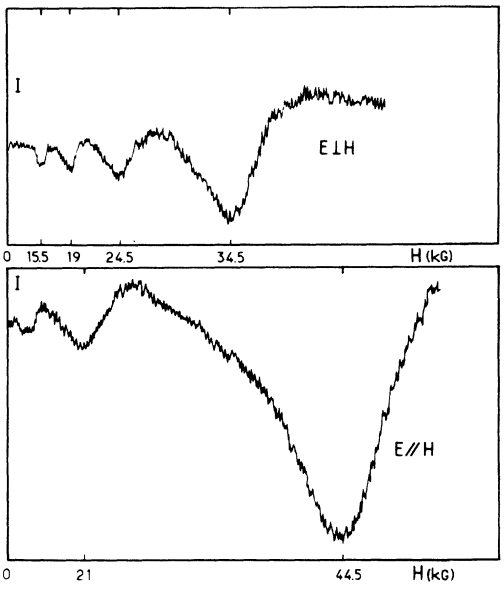

FIG. 2. Transmitted intensity vs magnetic field at $h\nu = 334$ meV in the Voigt configuration. The magnetic field is in an arbitrary direction of the (111) plane.

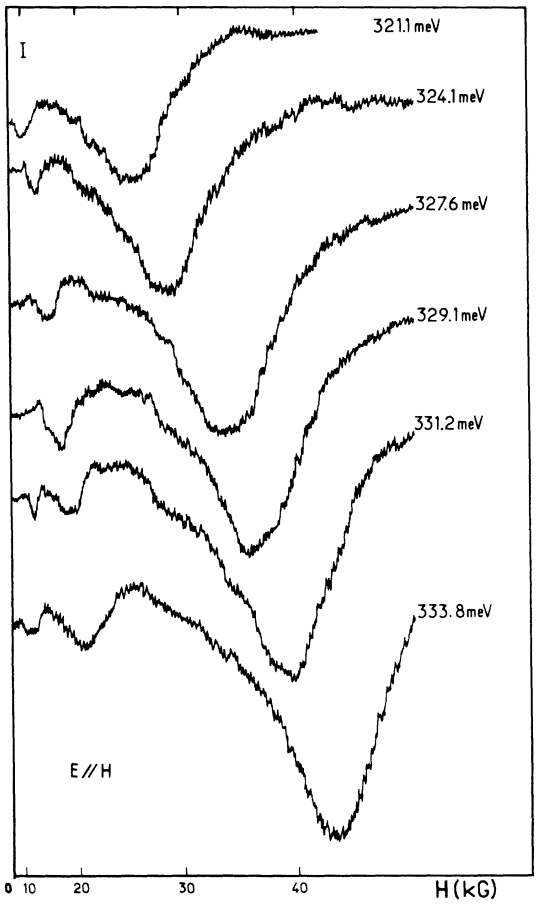

FIG. 3. Variation of the transmitted intensity vs magnetic field at various photon energies, in the Voigt configuration ($\vec{\epsilon} \parallel \vec{H}$).

II. EXPERIMENTAL RESULTS

Recorder traces of the transmitted intensity at fixed energies as a function of the magnetic field are reported in Figs. 2–6. In the Voigt configuration ($\vec{\epsilon} \parallel \vec{H}$ and $\vec{\epsilon} \perp \vec{H}$) (Figs. 2 and 3), the magnetic field is oriented in an arbitrary direction of the (111) plane. σ^+ and σ^- spectra, obtained for $\vec{H} \parallel [111]$, are shown in Figs. 4–6.

Energies of the transmission minima versus the magnetic field strength for the different polarizations are reported in Fig. 7.

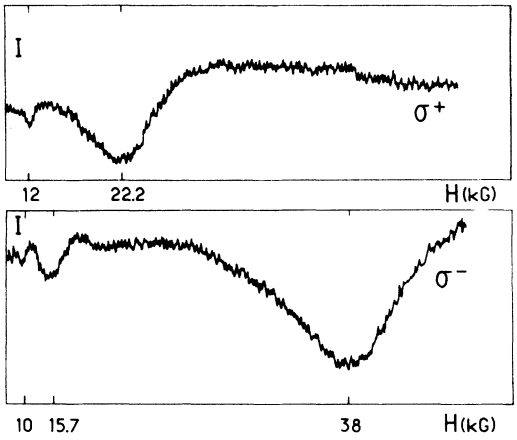

FIG. 4. Transmitted intensity vs magnetic field at $h\nu = 323$ meV in the Faraday configuration $\vec{H} \| [111]$.

III. THEORETICAL ANALYSIS OF RESULTS

The analysis of experimental results is carried out by calculating intensities and energies of the interband magneto-optical transitions. The lines observed for each polarization are identified. The valence- and conduction-band parameters are determined by fitting the computed energies with the experimental lines.

This analysis is made by using simplified descriptions of Γ_6 and Γ_8 magnetic levels: (i) A first approximation consists of applying the theory of

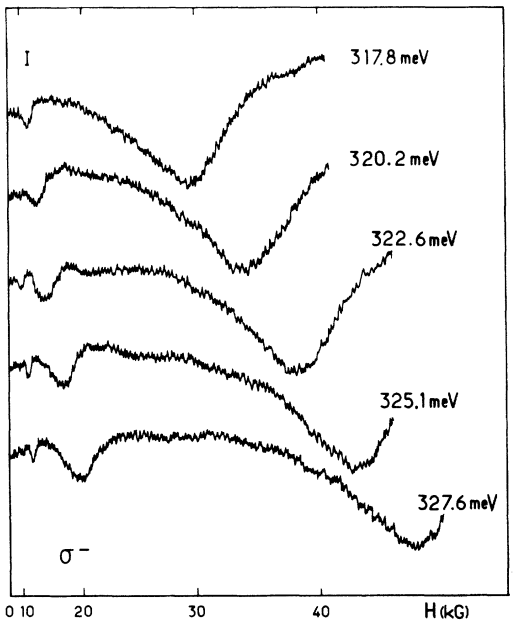

FIG. 5. Variation of the transmitted intensity vs magnetic field at various photon energies in the Faraday configuration for σ^- polarization: $\vec{H} \| [111]$.

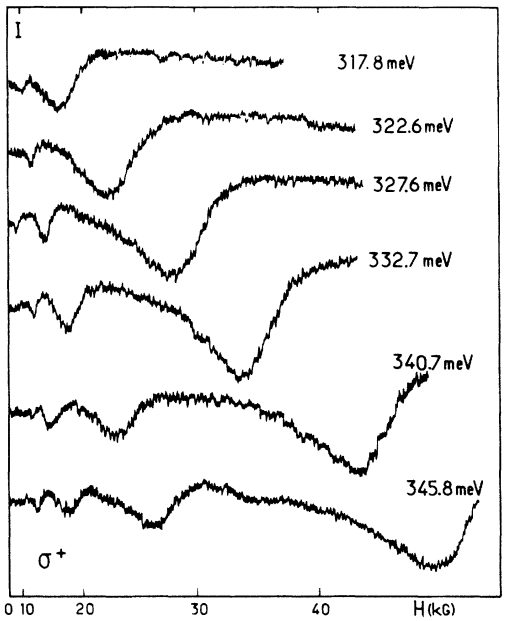

FIG. 6. Variation of the transmitted intensity vs magnetic field at various photon energies in the Faraday configuration for σ^+ polarization: $\vec{H} \| [111]$.

Luttinger[7] to the degenerate Γ_8 bands. This treatment, which accounts for the quantum effects in the conduction band but does not describe the effects of

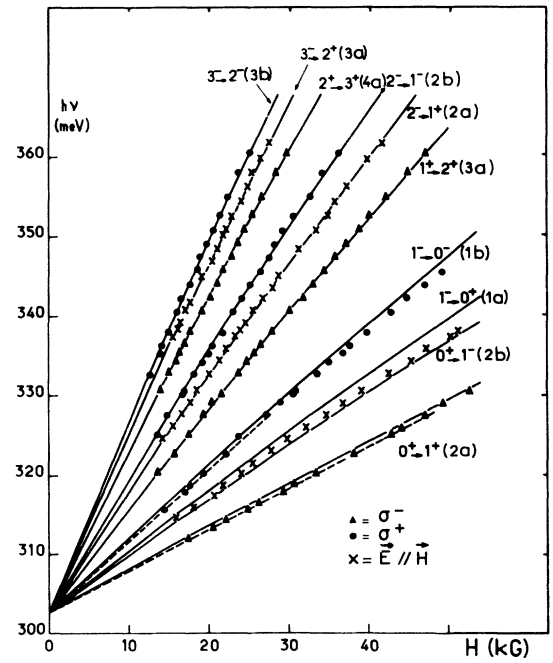

FIG. 7. Magnetic field dependence of σ^+, σ^-, and $\vec{\epsilon} \| \vec{H}$ transition energies. Dots are experimental data. Lines represent the theoretical variations computed using both the three-band model (solid lines) and the Luttinger theory (dashed lines).

nonparabolicity, is applicable for analyzing lines observed in the low-energy region ($\hbar\omega - \epsilon_0 < 30$ meV), involving transitions in the first quantum electronic levels. (ii) The simplified theory of the "three-band model"[8,9] is used to describe the effects of nonparabolicity observed in the high-energy region. This approximation, which neglects the quantum effects in Γ_8, is applied to analyze the transitions involving high electronic Landau levels.

A. Parabolic Range

1. Γ_8 *Magnetic Levels*

In the absence of magnetic field, Γ_8 is a fourfold-degenerate band. The band-edge Bloch functions $u_{j0}(j=1,\cdots,4)$ in the (J, m_J) representation are:

$$\begin{aligned} u_{10}(\tfrac{3}{2},\tfrac{3}{2}) &= \sqrt{\tfrac{1}{2}}\,(X+iY)\uparrow\,, \\ u_{20}(\tfrac{3}{2},-\tfrac{1}{2}) &= \sqrt{\tfrac{1}{6}}\,(X-iY)\uparrow+\sqrt{\tfrac{2}{3}}\,Z\downarrow\,, \\ u_{30}(\tfrac{3}{2},\tfrac{1}{2}) &= -\sqrt{\tfrac{1}{6}}\,(X+iY)\downarrow+\sqrt{\tfrac{2}{3}}\,Z\uparrow\,, \\ u_{40}(\tfrac{3}{2},-\tfrac{3}{2}) &= \sqrt{\tfrac{1}{2}}\,(X-iY)\downarrow\,. \end{aligned} \tag{1}$$

Magnetic levels are obtained by applying the theory of Luttinger and Kohn[10] and Luttinger.[7] The zero-order wave functions are

$$\Psi(\vec{r}) = \sum_j F_j(\vec{r})\,u_{j0}(\vec{r})\,. \tag{2}$$

The envelope functions F_j and the energies are the solutions of the four coupled equations:

$$\sum_{j'}[D_{jj'}(\vec{P}) - E\delta_{jj'}]F_{j'}(\vec{r}) = 0\,, \tag{3}$$

where $D_{jj'}$ is the quadratic function of $\vec{P} = -i\vec{\nabla} + e\vec{A}/\hbar c$:

$$D_{jj'}(\vec{P}) = \frac{\hbar^2 P^2}{2m}\,\delta_{jj'} + \frac{\hbar^2}{m^2}\sum_{\mu\neq j,j'}\frac{\vec{P}\cdot\vec{\Pi}_{j\mu}(0)\vec{P}\cdot\vec{\Pi}_{\mu j'}(0)}{E_j(0)-E_\mu(0)}\,;$$

j, j' run over the four degenerate states and μ over all bands, excluding Γ_8. $E_j(0)$ is the energy of the degenerate set and $E_\mu(0)$ is the energy of the μth unperturbed state. $\vec{\Pi}_{j\mu}$ is the interband matrix element:

$$\vec{\Pi}_{j\mu}(0) = \frac{(2\pi)^3}{\Omega}\int_{\text{cell}} u^*_{j0}(\vec{r}) \times\left(\frac{\hbar\vec{\nabla}}{i} + \frac{\hbar}{4mc^2}\,\vec{\sigma}\,\Lambda\overrightarrow{\nabla V}\right)u_{\mu 0}(\vec{r})\,d\vec{r}\,,$$

where V is the periodic potential and σ is the Pauli spin vector. Using group theory, Luttinger[7] has derived the form of the $D_{jj'}$ matrix Hamiltonian for the degenerated valence band of germanium, and has given an exact solution for a magnetic field in the [111] direction. This result is applicable to the degenerated Γ_8 band of HgTe, if we neglect the existence of linear k terms arising from the lack of inversion symmetry in the zinc-blende lattice. We will only consider the orientation of the magnetic field along [111], which corresponds to experimental data obtained in the Faraday geometry with circularly polarized light. In addition, we will neglect warping ($\gamma_2 = \gamma_3 = \bar{\gamma}$) and q parameter. The Hamiltonian matrix D, written in terms of the 4×4 J_x, J_y, J_z angular momentum matrices (for a state of spin $\frac{3}{2}$), is[7,11]

$$\begin{aligned} D = -\frac{\hbar^2}{m}\Big\{ &(\gamma_1+\tfrac{5}{2}\bar{\gamma})\frac{P^2}{2} - \bar{\gamma}(P_x^2J_x^2 + P_y^2J_y^2 + P_z^2J_z^2 \\ &+ 2\{P_xP_y\}\{J_xJ_y\} + 2\{P_xP_z\}\{J_xJ_z\} \\ &+ 2\{P_yP_z\}\{J_yJ_z\}) + \frac{eH}{c\hbar}\kappa J_z\Big\}\,. \end{aligned} \tag{4}$$

P_x, P_y, P_z represent the components of the operator $\vec{P}$ along the trirectangle coordinates system x, y, z, with the z axis aligned in the magnetic field direction. By expressing the transverse components of the momentum P_x and P_y in terms of a and $a^\dagger$ operators $a^\dagger = (\hbar c/2eH)^{1/2}(P_x + iP_y)$ and $a = (\hbar c/2eH)^{1/2} \times (P_x - iP_y)$, D becomes[11,12]:

$$D = -\frac{eH\hbar}{mc}\begin{vmatrix} (\gamma_1+\bar{\gamma})(a^\dagger a+\frac{1}{2})+\frac{3}{2}\kappa \\ +\frac{1}{2}(\gamma_1-2\bar{\gamma})P_H^2 & -\sqrt{3}\,\bar{\gamma}a^2 & -\sqrt{6}\,\bar{\gamma}aP_H & 0 \\ -\sqrt{3}\,\bar{\gamma}a^{\dagger 2} & (\gamma_1-\bar{\gamma})(a^\dagger a+\frac{1}{2})-\frac{1}{2}\kappa \\ & +\frac{1}{2}(\gamma_1+2\bar{\gamma})P_H^2 & 0 & \sqrt{6}\,\bar{\gamma}aP_H \\ -\sqrt{6}\,\bar{\gamma}a^\dagger P_H & 0 & (\gamma_1-\bar{\gamma})(a^\dagger a+\frac{1}{2})+\frac{1}{2}\kappa \\ & & +\frac{1}{2}(\gamma_1+2\bar{\gamma})P_H^2 & -\sqrt{3}\,\bar{\gamma}a^2 \\ 0 & \sqrt{6}\,\bar{\gamma}a^\dagger P_H & -\sqrt{3}\,\bar{\gamma}a^{\dagger 2} & (\gamma_1+\bar{\gamma})(a^\dagger a+\frac{1}{2})-\frac{3}{2}\kappa \\ & & & +\frac{1}{2}(\gamma_1-2\bar{\gamma})P_H^2 \end{vmatrix}\,, \tag{5}$$

where $P_H = (\hbar c/eH)^{1/2} P_z$. As interband transitions occur at $k_z = 0$, we first consider the solution of the effective-mass equation (3) for $P_H = 0$. The magnetic levels split into $a(m_J = \frac{3}{2}, -\frac{1}{2})$ and $b(m_J = \frac{1}{2}, -\frac{3}{2})$ sets.

The *wave functions* are a combination of the n and n-2 harmonic oscillator functions f:

$$\Psi_{a,n} = \begin{vmatrix} a_{1n} & f_{n-2} \\ a_{2n} & f_n \end{vmatrix} \begin{vmatrix} u_{3/2} \\ u_{-1/2} \end{vmatrix} , \tag{6}$$

$$\Psi_{b,n} = \begin{vmatrix} b_{1n} & f_{n-2} \\ b_{2n} & f_n \end{vmatrix} \begin{vmatrix} u_{1/2} \\ u_{-3/2} \end{vmatrix} . \tag{7}$$

Energies of a and b sets are $E^{\pm}_{a,b}(n) = (-eH\hbar/mc) \times \epsilon^{\pm}_{a,b}(n)$

$$a \text{ set: } \begin{cases} \epsilon^{\pm}_a(n) = \gamma_1(n - \frac{1}{2}) - \bar{\gamma} + \frac{1}{2}\kappa \\ \qquad \pm \{[\bar{\gamma}(n - \frac{1}{2}) - \gamma_1 + \kappa]^2 + 3\bar{\gamma}^2 n(n-1)\}^{1/2} \\ \qquad \text{for } n \geq 2 , \\ \epsilon_a(1) = \frac{3}{2}(\gamma_1 - \bar{\gamma}) - \frac{1}{2}\kappa , \\ \epsilon_a(0) = \frac{1}{2}(\gamma_1 - \bar{\gamma}) - \frac{1}{2}\kappa . \end{cases} \tag{8}$$

The coefficients a_{1n}, a_{2n} in (6) are the solutions of the equations

$$a_{1n}\bar{\gamma}[3n(n-1)]^{1/2} = a_{2n}[(\gamma_1 - \bar{\gamma})(n + \tfrac{1}{2}) - \tfrac{1}{2}\kappa - \epsilon^{\pm}_a(n)] ,$$
$$a_{1n}^2 + a_{2n}^2 = 1 , \quad n \geq 2 . \tag{9}$$

For $n = 0, 1$, $a_1 = 0$ and $a_2 = 1$.

$$b \text{ set: } \begin{cases} \epsilon^{\pm}_b(n) = \gamma_1(n - \frac{1}{2}) + \bar{\gamma} - \frac{1}{2}\kappa \\ \qquad \pm \{[\bar{\gamma}(n - \frac{1}{2}) + \gamma_1 - \kappa]^2 + 3\bar{\gamma}^2 n(n-1)\}^{1/2} , \\ \epsilon_b(1) = \frac{3}{2}(\gamma_1 + \bar{\gamma}) - \frac{3}{2}\kappa , \\ \epsilon_b(0) = \frac{1}{2}(\gamma_1 + \bar{\gamma}) - \frac{3}{2}\kappa . \end{cases} \tag{10}$$

b_{1n} and b_{2n} in (7) are given by

$$b_{1n}\bar{\gamma}[3n(n-1)]^{1/2} = b_{2n}[(\gamma_1 + \bar{\gamma})(n + \tfrac{1}{2}) - \tfrac{3}{2}\kappa - \epsilon^{\pm}_b(n)] ,$$
$$b_{1n}^2 + b_{2n}^2 = 1 , \quad n \geq 2 . \tag{11}$$

For $n = 0, 1$, $b_1 = 0$ and $b_2 = 1$. By solving the four coupled equations for $P_H \neq 0$, the dependence upon k_H of the energy levels is obtained. The results are presented in Sec. III A 4. The electronic levels are described by $\epsilon_{a,b}(1)$ and $\epsilon^{-}_{a,b}(n)$. The holes correspond to $\epsilon_{a,b}(0)$ and $\epsilon^{+}_{a,b}(n)$.

2. *Interband $\Gamma_6 \to \Gamma_8$ Magneto-optical Transitions*

At the center of the zone, Γ_6 is a simple band with spherical symmetry. The magnetic levels associated with the two spin states $(m_s = \pm\frac{1}{2})$ are described by the wave functions

$$\Psi^{+} = f_{n'}(\vec{r})\,|iS\uparrow\rangle , \quad \Psi^{-} = f_{n'}(\vec{r})\,|iS\downarrow\rangle . \tag{12}$$

The energies are (at $k_z = 0$)

$$E^{\pm}_{\Gamma_6}(n') = -\epsilon_0^{-}(n' + \tfrac{1}{2})\frac{eH\hbar}{m_v c} \mp \tfrac{1}{2} g_v \mu_B H , \tag{13}$$

where m_v and g_v represent the band-edge effective mass and gyromagnetic factor and $\epsilon_0 = E_{\Gamma_8} - E_{\Gamma_6}$. The selection rules and transition probabilities are obtained by evaluating interband matrix elements.[13] From (1), (6), (7), and (12) we find

$$\langle \Psi_a^{-} | \vec{\epsilon} \cdot \vec{P} | \Psi^{+}_{\Gamma_6} \rangle = i \langle Z | P_z | S \rangle \times \{\epsilon^{-}\sqrt{\tfrac{1}{2}}\, a^{-}_{1n}\, \delta_{n',n-2} + \epsilon^{+}\sqrt{\tfrac{1}{6}}\, a^{-}_{2n}\, \delta_{n',n}\} ,$$
$$\langle \Psi_a^{-} | \vec{\epsilon} \cdot \vec{P} | \Psi^{-}_{\Gamma_6} \rangle = i \langle Z | P_z | S \rangle\, \epsilon_z \sqrt{\tfrac{2}{3}}\, a^{-}_{2n}\, \delta_{n,n'} ,$$
$$\langle \Psi_b^{-} | \vec{\epsilon} \cdot \vec{P} | \Psi^{-}_{\Gamma_6} \rangle = i \langle Z | P_z | S \rangle \times \{\epsilon^{+}\sqrt{\tfrac{1}{2}}\, b^{-}_{2n}\, \delta_{n,n'} - \epsilon^{-}\sqrt{\tfrac{1}{6}}\, b^{-}_{1n}\, \delta_{n',n-2}\} ,$$
$$\langle \Psi_b^{-} | \vec{\epsilon} \cdot \vec{P} | \Psi^{+}_{\Gamma_6} \rangle = i \langle Z | P_z | S \rangle\, \epsilon_z\, b^{-}_{1n} \sqrt{\tfrac{2}{3}}\, \delta_{n',n-2} ,$$
$$\epsilon^{\pm} = \epsilon_x \pm i\epsilon_y .$$

Interband magneto-optical transitions for different polarizations are listed in Table I. From the relative amplitudes of the coefficients a_n and b_n, given by (9) and (11), predominant $\epsilon^{+}, \epsilon^{-}$ transitions are

$$(n-2, \tfrac{1}{2}) \to a^{-}(n) \text{ for } \epsilon^{-} ,$$
$$(n, -\tfrac{1}{2}) \to b^{-}(n) \text{ for } \epsilon^{+} .$$

3. *Comparison with Experimental Results*

The theoretical data enable us to identify the observed transitions and to determine the valence and conduction band parameters. The identification of the lines is reported in Figure 7.

A quantitative comparison is made between the experimental positions of the lines (for circular polarization) with the theoretical energies (Table I). From the slopes of the linear variation $E(H)$, observed in the low-energy range, we determine the Luttinger parameters γ_1, $\bar{\gamma}$, κ, the band-edge effective mass, and the g factor of the light holes. The determination of Γ_8 parameters is carried out by taking into account the experimental data of electron cyclotron resonance and electric spin resonance obtained by Tuchendler, Grynberg, Couder, and Thomé (reported in the following paper[6]). The cyclotron-resonance line in the Faraday geometry $(\vec{\epsilon} \perp \vec{H})$ corresponds to $a(1) \to a^{-}(2)$, the spin-resonance line to $a(1) \to b(1)$.

The set of parameters, which interpret energies of both intraband and interband transitions, observed in the same field range is

$$\Gamma_8: \begin{cases} \gamma_1 = -12.8 \pm 0.5 , \\ \bar{\gamma} = -8.4 \pm 0.1 , \\ \kappa = -10.5 \pm 0.3 , \end{cases} \tag{14}$$

TABLE I. Interband magneto-optical transitions for different polarizations.

Allowed transition	Relative transition probabilities: Circular polarization ϵ^+	Circular polarization ϵ^-	Linear polarization $\vec{\epsilon} \parallel \vec{H}$	Energy transition
$(n, \frac{1}{2}) \rightarrow a^-(n)$	$\frac{1}{6}\lvert a^-_{2n}\rvert^2$	0		$\epsilon_0 + E^-_a(n) + (n+\frac{1}{2})\frac{eH\hbar}{m_v c} + \frac{1}{2}g_v\mu_B H$
$(n, -\frac{1}{2}) \rightarrow b^-(n)$	$\frac{1}{2}\lvert b^-_{2n}\rvert^2$	0		$\epsilon_0 + E^-_b(n) + (n+\frac{1}{2})\frac{eH\hbar}{m_v c} - \frac{1}{2}g_v\mu_B H$
$(n-2, \frac{1}{2}) \rightarrow a^-(n)$	0	$\frac{1}{2}\lvert a^-_{1n}\rvert^2$		$\epsilon_0 + E^-_a(n) + (n-\frac{3}{2})\frac{eH\hbar}{m_v c} + \frac{1}{2}g_v\mu_B H$
$(n-2, -\frac{1}{2}) \rightarrow b^-(n)$	0	$\frac{1}{6}\lvert b^-_{1n}\rvert^2$		$\epsilon_0 + E^-_b(n) + (n-\frac{3}{2})\frac{eH\hbar}{m_v c} - \frac{1}{2}g_v\mu_B H$
$(n-2, \frac{1}{2}) \rightarrow b^-(n)$	0	0	$\frac{1}{3}\lvert b^-_{1n}\rvert^2$	$\epsilon_0 + E^-_b(n) + (n-\frac{3}{2})\frac{eH\hbar}{m_v c} + \frac{1}{2}g_v\mu_B H$
$(n, -\frac{1}{2}) \rightarrow a^-(n)$	0	0	$\frac{1}{3}\lvert a^-_{2n}\rvert^2$	$\epsilon_0 + E^-_a(n) + (n+\frac{1}{2})\frac{eH\hbar}{m_v c} - \frac{1}{2}g_v\mu_B H$

$$\Gamma_6:\begin{cases} m_v/m_0 = 0.028 \pm 0.001 \ , \\ g_v = -41 \pm 4 \ . \end{cases}$$

Figure 8 represents a schematic diagram of magnetic levels at $k_H = 0$, and interband transitions for the different polarizations.

4. K_z Dependence of Γ_8 Magnetic Levels

For $P_H \neq 0$, the envelope wave function solutions of the matrix Hamiltonian (5) are of the form

$$\Psi_m = \begin{vmatrix} c_{1m} f_{m-2} \\ c_{2m} f_m \\ c_{3m} f_{m-1} \\ c_{4m} f_{m+1} \end{vmatrix} \ .$$

The variation upon k_z of the energies $\epsilon^{\pm}_{a,b}$ is determined by solving the determinant equation:

$$\begin{vmatrix} (\gamma_1+\bar{\gamma})(m-\frac{3}{2})+\frac{3}{2}\kappa \\ +\frac{1}{2}(\gamma_1-2\bar{\gamma})L^2k_z^2-\epsilon & -[3m(m-1)]^{1/2}\bar{\gamma} & -[6(m-1)]^{1/2}Lk_z\bar{\gamma} & 0 \\ -[3m(m-1)]^{1/2}\bar{\gamma} & (\gamma_1-\bar{\gamma})(m+\frac{1}{2})-\frac{1}{2}\kappa \\ +\frac{1}{2}(\gamma_1+2\bar{\gamma})L^2k_z^2-\epsilon & 0 & [6(m+1)]^{1/2}\bar{\gamma}Lk_z \\ -[6(m-1)]^{1/2}\bar{\gamma}Lk_z & 0 & (\gamma_1-\bar{\gamma})(m-\frac{1}{2})+\frac{1}{2}\kappa \\ +\frac{1}{2}(\gamma_1+2\bar{\gamma})L^2k_z^2-\epsilon & -[3m(m+1)]^{1/2}\bar{\gamma} \\ 0 & [6(m+1)]^{1/2}\bar{\gamma}Lk_z & -[3m(m+1)]^{1/2}\bar{\gamma} & (\gamma_1+\bar{\gamma})(m+\frac{3}{2})-\frac{3}{2}\kappa \\ & & & +\frac{1}{2}(\gamma_1-2\bar{\gamma})L^2k_z^2-\epsilon \end{vmatrix} = 0 \ , \qquad (15)$$

where $L^2 = \hbar c/eH$. The analytical form $\epsilon(k_z)$ is only derived for the first quantum levels:

$$\epsilon_b(0) = \tfrac{1}{2}(\gamma_1+\bar{\gamma}) - \tfrac{3}{2}\kappa + \tfrac{1}{2}(\gamma_1-2\bar{\gamma})L^2k_z^2 \ ,$$

$$\epsilon_a(0) = \gamma_1 + \tfrac{1}{2}\bar{\gamma} - \kappa + \tfrac{1}{2}\gamma_1 L^2k_z^2 + [(-\tfrac{1}{2}\gamma_1 - \bar{\gamma} + \tfrac{1}{2}\kappa + \bar{\gamma}L^2k_z^2)^2 + 6\bar{\gamma}^2L^2k_z^2]^{1/2} \ ,$$

$$\epsilon_b(1) = \gamma_1 + \tfrac{1}{2}\bar{\gamma} - \kappa + \tfrac{1}{2}\gamma_1 L^2k_z^2 - [(-\tfrac{1}{2}\gamma_1 - \bar{\gamma} + \tfrac{1}{2}\kappa + \bar{\gamma}L^2k_z^2)^2 + 6\bar{\gamma}^2L^2k_z^2]^{1/2} \ .$$

For the higher levels, the variation of the energy, as a function of $P_H = Lk_z$, was computed for the values of parameters ($\gamma_1 = -12.8$, $\bar{\gamma} = -8.4$, $\kappa = -10.5$) previously obtained. Figure 9 presents the calculated variations $\epsilon^{\pm}_{a,b}(k_z)$. The set of holes $\epsilon^{+}_{a,n}(k_z)$ exhibits a nonmonotonic dependence for $n \geq 2$. Energy maxima occur for $P_z = \pm LK_m \neq 0$. For $n = 2$, $LK_m = 0.9$ and for $n = 3$, $LK_m = 0.8$. The energy distance between the maxima and $k_z = 0$ point is relatively small: $\epsilon^{+}_{a,n}(LK_m) - \epsilon^{+}_{a,n}(0) = 0.24$ meV/T for $n = 2$ and 0.17 meV/T for $n = 3$. The detail of the structure of the first level of holes near $k_z = 0$ is reported in Fig. 10. Similar calculations were recently performed by Zawadzki.[14]

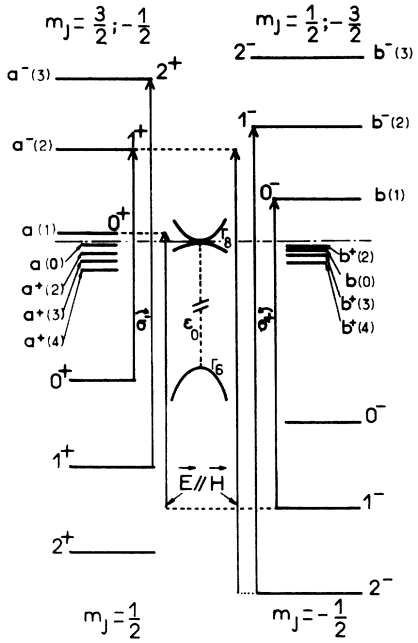

FIG. 8. Scheme of Γ_8 and Γ_6 magnetic levels at $k_H = 0$ and σ^+, σ^-, and $\vec{\epsilon} \| \vec{H}$ interband transitions.

B. Nonparabolic Range

1. *Interband Magneto-optical Transitions*

The analysis of the experimental results obtained in the whole investigated energy range is made by

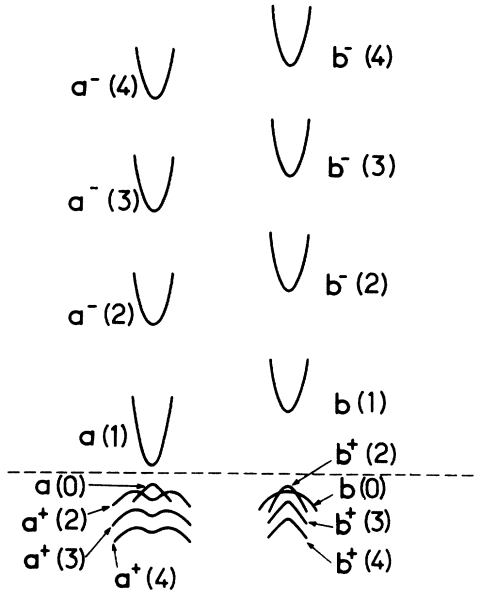

FIG. 9. P_H dependence of electrons and heavy holes magnetic levels for $\vec{H} \| [111]$. Energies are calculated by solving the determinant equation (15) for the set of parameters (14).

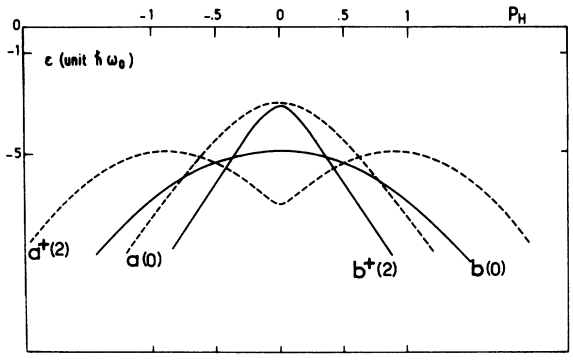

FIG. 10. Structure of the first heavy holes magnetic levels for $\vec{H} \| [111]$. Energies are plotted vs $P_H = Lk_H$.

using a theoretical description of Γ_6 and Γ_8 magnetic levels derived in the "three-band approximation". This simplified procedure, developed by Yafet[9] and Kacman and Zawadzki[8] in the case of InSb and α-Sn-type materials, includes the $\vec{k} \cdot \vec{p}$ interaction between Γ_6-Γ_7-Γ_8 levels, neglecting higher bands. As Luttinger effects are not included, this approach is only valid to describe electronic levels of high quantum number.

In the energy range $\epsilon \ll \frac{2}{3}\Delta (\Delta = E_{\Gamma_8} - E_{\Gamma_7} \simeq 1$ eV), the electron- and light-hole energies are approximately given by

$$(\Gamma_8): \quad E_N^{\pm} = -\tfrac{1}{2}\epsilon_0 + [(\tfrac{1}{2}\epsilon_0)^2 + \epsilon_0 D_N^{\pm}]^{1/2} ,$$

$$(\Gamma_6): \quad E_{N'}^{\pm} = -\tfrac{1}{2}\epsilon_0 - [(\tfrac{1}{2}\epsilon_0)^2 + \epsilon_0 D_{N'}^{\pm}]^{1/2} ,$$

$$D_N^{\pm} = \frac{eH\hbar}{m^*c}(N + \tfrac{1}{2}) \pm \tfrac{1}{2} g^* \mu_B H + \frac{\hbar^2 k_z^2}{2m^*} .$$

m^*, g^* are the band-edge effective mass and the gyromagnetic factor, respectively. For electronic levels, + and − sets correspond respectively to a and b ladders of the Luttinger notation and $N = n - 1$ (Fig. 8).

Using the analytical form of the wave functions $\Psi_N^{\pm}$ derived by Kacman and Zawadzki,[8] the interband matrix elements are evaluated for $k_z = 0$. The results are presented in Table II, where

$$|a_N^{\pm}|^2 = \frac{E_N^{\pm}(\Gamma_8)}{\epsilon_0 + 2E_N^{\pm}(\Gamma_8)} , \qquad |b_N^{\pm}|^2 = \frac{1}{3}\frac{\epsilon_0 + E_N^{\pm}(\Gamma_8)}{\epsilon_0 + 2E_N^{\pm}(\Gamma_8)} ,$$

$$|\alpha_{N'}^{\pm}|^2 = \frac{E_{N'}^{\pm}(\Gamma_6)}{\epsilon_0 + 2E_{N'}^{\pm}(\Gamma_6)} , \qquad |\beta_{N'}^{\pm}|^2 = \frac{\epsilon_0 + E_{N'}^{\pm}(\Gamma_6)}{\epsilon_0 + 2E_{N'}^{\pm}(\Gamma_6)} ,$$

$$\mathcal{K} = \frac{-i}{m} \langle S | p_z | Z \rangle .$$

Calculations of the transition probabilities indicate that the predominant transitions are

$$\begin{aligned} &\vec{\epsilon} \| \vec{H} , \quad N'^- \rightarrow N^+ , \quad N = N' - 1 , \\ &\epsilon^+ , \quad N'^- \rightarrow N^- , \quad N = N' - 1 , \\ &\epsilon^- , \quad N'^+ \rightarrow N^+ , \quad N = N' + 1 . \end{aligned} \tag{16}$$

TABLE II. Results of interband matrix elements evaluated at $k_z = 0$ using the analytical form of the wave functions $\Psi_N^{\pm}$ derived by Kacman and Zawadzki (Ref. 8).

Polarization	Allowed transition	Selection rules	Transition probabilities
$\vec{\epsilon} \parallel \vec{H}$	$N'^{+} \rightarrow N^{-}$	$N = N' + 1$	$(m\mathcal{K})^2 \frac{\hbar\omega^* N}{2} \left(\frac{\beta_N^+ a_N^-}{\sqrt{D_N^+}} - \frac{\alpha_N^+ b_N^-}{\sqrt{D_N^-}} \right)^2$
	$N'^{-} \rightarrow N^{+}$	$N = N' - 1$	$(m\mathcal{K})^2 \frac{\hbar\omega^* N'}{2} \left(\frac{\alpha_{N'}^- b_N^+}{\sqrt{D_N^+}} - \frac{a_N^+ \beta_{N'}^-}{\sqrt{D_{N'}^-}} \right)^2$
ϵ^{+}	$N'^{+} \rightarrow N^{+}$	$N = N' - 1$	$(m\mathcal{K})^2 \frac{N'\hbar\omega^*}{4} \left(\frac{3a_N^+ \beta_{N'}^+}{\sqrt{D_{N'}^+}} + \frac{\alpha_N^+ b_{N'}^+}{\sqrt{D_N^+}} \right)^2$
	$N'^{-} \rightarrow N^{-}$	$N = N' - 1$	$(m\mathcal{K})^2 \frac{N'\hbar\omega^*}{4} \left(\frac{3\alpha_{N'}^- b_N^-}{\sqrt{D_N^-}} + \frac{a_N^- \beta_{N'}^-}{\sqrt{D_{N'}^-}} \right)^2$
ϵ^{-}	$N'^{+} \rightarrow N^{+}$	$N = N' + 1$	$(m\mathcal{K})^2 \frac{N\hbar\omega^*}{4} \left(\frac{3\alpha_N^+ b_{N'}^+}{\sqrt{D_N^+}} + \frac{a_{N'}^+ \beta_N^+}{\sqrt{D_{N'}^+}} \right)^2$
	$N'^{-} \rightarrow N^{-}$	$N = N' + 1$	$(m\mathcal{K})^2 \frac{N\hbar\omega^*}{4} \left(\frac{3a_{N'}^- \beta_N^-}{\sqrt{D_{N'}^-}} + \frac{\alpha_{N'}^- b_N^-}{\sqrt{D_N^-}} \right)^2$

2. *Comparison with Experimental Data*

The identification of the lines is made according to the selection rules (16). For $\vec{\epsilon} \parallel \vec{H}$, the first transition $1^- \rightarrow 0^+$ is not expected to be observed as the 0^+ electronic level is populated. At 4.4 °K, the position of the Fermi level is about 4 meV above the Γ point. The experimental line should be assigned to $0^+ \rightarrow 1^-$, occuring for the same polarization (Table II). The energies of the different sets of transitions ($\vec{\epsilon} \parallel \vec{H}, \epsilon^+, \epsilon^-$) are computed as a function of the magnetic field and fitted to the positions of the lines. The best agreement between theoretical and experimental energies, shown in Fig. 7, is obtained for the following values of the parameters:

$\epsilon_0 = 302.5$ meV at 4.4 °K,

$$\Gamma_8: \begin{cases} \frac{m_e}{m_0} = 0.031 \pm 0.001 , \\ g_e = -22 \pm 4 , \end{cases} \qquad \Gamma_6: \begin{cases} \frac{m_v}{m_0} = 0.028 \pm 0.001 , \\ g_v = -41 \pm 4 . \end{cases}$$

These results provide evidence of assymmetrical Γ_6 and Γ_8 levels, which could be explained by the interaction with higher bands. The effects of nonparabolicity are fairly accounted for by the three-band model. For all transitions involving $N = 2, 3$ electron quantum levels, the magnetic field dependence of the energies is in excellent agreement with the theoretical variations. For the transitions involving the first electronic levels ($1^- \rightarrow 0^-, 0^+ \rightarrow 1^+$), the discrepancies between observed and calculated energies result from the existence of quantum effects in the Γ_8 band, which are neglected in the nonparabolic model. As was shown in Sec. III A 3, the analysis performed on the basis of the Luttinger theory interprets quantitatively the positions of these first lines (ϵ^+ and ϵ^-) (Fig. 7).

Γ_6 parameters determined by applying both theoretical approximations are quite consistent.

IV. CONCLUSION

We present the first observation of $\Gamma_6 \rightarrow \Gamma_8$ magnetoabsorption in HgTe. Magnetoreflectivity was previously investigated in the same energy region by Groves, Brown, and Pidgeon.[4] The magnetoabsorption spectrum is, however, more directly related to the energy spectrum of the crystal. The main difficulty in carrying out transmission experiments in the spectral range 300–400 meV arises from the large absorption background due to $\Gamma_8 \rightarrow \Gamma_8$ transitions, superimposed on the $\Gamma_6 \rightarrow \Gamma_8$ magnetoabsorption spectrum. Thus, very thin crystals were required for a direct observation of magneto-optical transitions. Resonance lines connected with $\Gamma_8 \rightarrow \Gamma_8$ magneto-optical transitions were not observed in our experiments. The width of the high quantum levels ($n > 50$ for $H = 10$ kG) involved in such transitions, at photon energies $\hbar\omega > \epsilon_0$, is sufficiently large to preclude any resonant structure. However, a theoretical treatment of the imaginary part of the dielectric constant in presence of applied magnetic field has not yet been made in order to estimate the influence of $\Gamma_8 \rightarrow \Gamma_8$ transitions on the response function in the investigated energy region.

Experimental results of $\Gamma_6 \rightarrow \Gamma_8$ magnetoabsorption are interpreted using both the simplified theory of the three-band model (including the nonparabolicity of the bands) and the Luttinger theory. By fitting transition energies in both models, Γ_6 band-edge effective mass and g factor and Luttinger parameters ($\gamma_1, \bar{\gamma}, \kappa$) for Γ_8 bands are evaluated. It is interesting to point out that the Luttinger parameters satisfactorily explain $\Gamma_8 \rightarrow \Gamma_8$ intraband and interband transitions reported in the following paper.[6] Such is not the case for the set of parameters obtained by Groves *et al.*[4] The energy $E_p = 2m\mathcal{K}^2 = 18 \pm 1$ eV, obtained from magnetoreflection experiments at 30 °K by Groves *et al.*,[4] is appreciably higher than the value deduced from our parameters: $E_p = 15.5 \pm 1$ eV at 4.4 °K.

The band-edge effective masses of electrons and heavy holes are described by γ_1 and $\bar{\gamma}$ for large n. Heavy holes effective mass deduced from our results is about 1.5 times smaller than the value obtained from galvanomagnetic measurements on p-type HgTe.[15] The origin of such a difference can probably result from the complex structure of heavy holes magnetic levels, reported in the present paper, or also from our oversimplification of the band structure. Our analysis neglects the warping and the linear k term arising from the lack of inversion symmetry. Our experimental data show that warping exists, but is probably not important in HgTe: energies of $\vec{\epsilon} \perp \vec{H}$ transitions observed for $\vec{H} \parallel [111]$ and for different orientations of the field in the (111) plane are slightly shifted.

The existence of linear k terms can drastically

modify the k_z dependence of Landau levels, particularly for heavy holes. There is still no evidence concerning the magnitude of the linear term, which will probably be evaluated from experiments that we are presently carrying out on p-type HgTe.

If warping and linear k terms are taken into consideration, a small modification of the electron magnetic levels is expected. The most striking effect would be the existence of new allowed transitions, induced by the change in the symmetry wave functions. These effects will be discussed in a future paper.

[1]S. H. Groves and W. Paul, in *Proceedings of the International Conference on the Physics of Semiconductors* (Dunod, Paris, 1964), p. 41.
[2]R. Piotrzkowski, S. Porowki, Z. Dziuba, J. Ginter, W. Giriat, and L. Sosnowski, Phys. Status Solidi **8**, K135 (1965).
[3]A. Mycielski and R. R. Galazka, in *Proceedings of the International Conference on the Physics of Semiconductors*, Moscow, 1968 (Nauka, Leningrad, 1968), p. 875.
[4]S. H. Groves, R. N. Brown, and C. R. Pidgeon, Phys. Rev. **161**, 779 (1967).
[5]C. R. Pidgeon and S. H. Groves, in *Conference on the II-VI Semiconducting Compounds*, edited by D. G. Thomas (Benjamin, New York, 1967), p. 1080.
[6]J. Tuchendler, M. Grynberg, Y. Couder, H. Thome, and R. Le Toullec, following paper, Phys. Rev. B 8, 3884 (1973).
[7]J. M. Luttinger, Phys. Rev. **102**, 1030 (1956).
[8]P. Kacman and W. Zawadzki, Phys. Status Solidi **47**, 629 (1971).
[9]Y. Yafet, Phys. Rev. **115**, 1172 (1959).
[10]J. M. Luttinger and W. Kohn, Phys. Rev. **97**, 869 (1955).
[11]J. J. Stickler, H. J. Zeiger, and G. S. Heller, Phys. Rev. **127**, 1077 (1962).
[12]R. R. Goodman, Phys. Rev. **122**, 397 (1961).
[13]L. Roth, B. Lax, and S. Zwerdling, Phys. Rev. **114**, 90 (1959).
[14]W. Zawadzki (private communication).
[15]V. I. Ivanov-Omskii, B. T. Kolomiets, Yu. F. Markov, A. Sh. Mekhtiev, and K. P. Smekalova, Fiz. Tekh. Poluprovodn. 1, 1442 (1967) [Sov. Phys.-Semicond. 1, 1203 (1967)].